Experimental Investigation of Lift and Drag Characteristics of a Typical MAV under Propeller Induced Flow

Arivoli Durai*
Experimental Aerodynamics Division, National Aerospace Laboratories, Bangalore, Karnataka 560037, India.

[Received date; Accepted date] – to be inserted later

Abstract
Experiments were conducted on a micro air vehicle (MAV) model in a low speed wind tunnel to study the actual lift and drag experienced by the model under propeller induced flow by ostracizing the thrust force generated by the propeller by decoupling the motor-propeller from the model and mounting it on a separate arrangement with minimal flow interference. Tests were conducted on the model at actual flight conditions - at a freestream velocity of 9 m/s (Re = 135000 based on root chord) with the propeller running at 8000 rpm. The lift and drag coefficients obtained from the model with decoupled motor-propeller arrangement are compared to those obtained from the model with attached motor-propeller for the same test conditions and justification is made in favor of the former method. Effects of propeller induced flow with respect to increase in propeller rpm on the lift and drag characteristics of the model were also studied. Higher C_L at higher angle of attack and increased C_D were observed for the model under propeller induced flow. With increase in propeller rpm, the effects seen in C_L and C_D are increased further.

NOMENCLATURE

C_L	lift coefficient
C_D	drag coefficient
L/D	lift-to-drag ratio
Re	Reynolds number
rpm	rotation per minute
V_∞	freestream velocity
α	angle of attack (degree)

1. INTRODUCTION

Researches in the field of MAVs are active for a long time, yet understanding of its aerodynamics are more challenging in certain aspects. A plethora of literature exist on the aerodynamic investigation of MAVs but very few literature [1-3, 6-9] are available which addresses the aerodynamics of MAVs under propeller induced flow. Null, Noseck and Shkarayev [1] in their attempt to study the effects of propeller induced flow on the aerodynamics of MAV, adopted a test methodology in which the dynamic thrust data were collected at the test velocity from the motor/propeller mounted on a pylon at 0^o angle of attack and the data was resolved into horizontal and vertical component for all the angles of attack the propelled MAV model was tested. To decouple the direct forces created by the propeller on the total lift and drag measured on MAV model, the vertical component contributing to overall lift is subtracted from the lift data and the horizontal component contributing to forward thrust is added to the total drag data of the propelled MAV model. The results obtained shows that the propeller induced flow caused higher magnitudes of lift at higher angles of attack & delayed stall, but a detrimental effect on the drag coefficients, and a subsequent decrease in the lift-to-drag ratio at low angles of attack. However, they concluded that, due to the way the aerodynamic coefficients were calculated, the effects in the

*Scientist, d.arivoli@nal.res.in

aerodynamic coefficients are partly a mathematical phenomenon.

Experiments by Gamble and Reeder [2] on a MAV to study the propeller-wing interaction were conducted in a static environment and also in wind tunnel. In static test, the motor/propeller was mounted on a separate torque/load cell and the wing/fuselage was mounted on a six-component balance, hence the propeller thrust and torque along with forces and moments acting on the wing/fuselage were measured. The result shows that between 12 and 18% of propeller thrust translates into airframe drag, with the largest percentage occurring for the wing placement closest to the propeller. While in a wind tunnel test the separation of the motor from the fuselage and wing was not implemented due to interference and blockage effects of the support, hence the motor-propeller was mounted on the nose of the fuselage and the test data has the aircraft drag and propeller thrust combined into a single reading and the motor torque and reaction roll moment combined into another single reading. Experimental studies conducted by Arivoli et al. [3] to investigate the propeller-induced flow on a thin cambered wing MAV also used the resultant global axial force (which is the difference of thrust and axial force measured by the balance) to calculate the lift and drag. In the previous studies, it was clearly shown that the thrust generated by the propeller hinders the actual measurement of axial force experienced by the model. Hence the only way to exclude thrust from the measurements is to decouple it to obtain meaningful lift and drag characteristics. Several works have been conducted in general aviation by decoupling the motor-propeller arrangement to exclude thrust from the measurements.

Work by Catalano [4] to study the effects of an installed propeller on wing aerodynamic characteristics of a pusher configuration used an experimental setup in which the propeller arrangement is decoupled from the wing. The wing was mounted on a force balance and the propeller was mounted on a separate pylon. The aerodynamic behavior of the wing was studied for different propeller positions. In a setup like this, the propeller thrust does not come into measurement made on the wing but the effect created by the propeller upstream on the wing is felt and measured. An arrangement like this does not produce any undesirable effects in measurements for a pusher configuration as the decoupled propeller arrangement was positioned downstream of the wing. However it's a different scenario for a tractor configuration as the decoupled propeller arrangement is placed in front of the wing which can cause undesirable flow interference.

Studies by Witkowski, Lee and Sullivan [5] to understand the aerodynamic interaction between propellers and wings for a tractor configuration used an experimental setup of mounting the propeller and wing separately inside the test section. The wing was mounted on a floor mounted six component balance and the propeller arrangement (in front of the wing) on a two-component electric strain gage balance. The setup was made in such a way to independently measure steady propeller and wing loads while minimizing the amount of undesirable interference from struts, shafts, and nacelles.

Adopting a similar testing approach for the MAV class of vehicles would shed more light into the understanding of the aerodynamics of the vehicle under propeller induced flow. Thus, the present work delineates a similar effort taken towards the understanding of aerodynamic behavior of a typical MAV model under propeller induced flow.

2. EXPERIMENTAL SETUP

2.1 Wind tunnel

Studies on the MAV model were undertaken in a 0.55 m x 0.55 m in-draft open circuit low speed wind tunnel. The tunnel is capable of generating freestream velocities in the range 3-50 m/sec. The present studies required flow velocity to be between 9 m/s, and so prior to undertaking the studies, the flow in the tunnel was calibrated in this velocity range to assess its uniformity and stability. The turbulence level in this speed range is observed to be less than 0.25% in the tunnel.

2.2 Model

Figure 1 shows geometric details of the MAV model. The span of the model is 300 mm and the root chord is 250 mm. The planform of the model is a modified version of inverse Zimmerman geometry as the wing tips are trimmed. The wing is based on Selig 4083 airfoil camber. The thickness and aspect ratio of the wing are 3 mm and 1.46 respectively. The fuselage is a

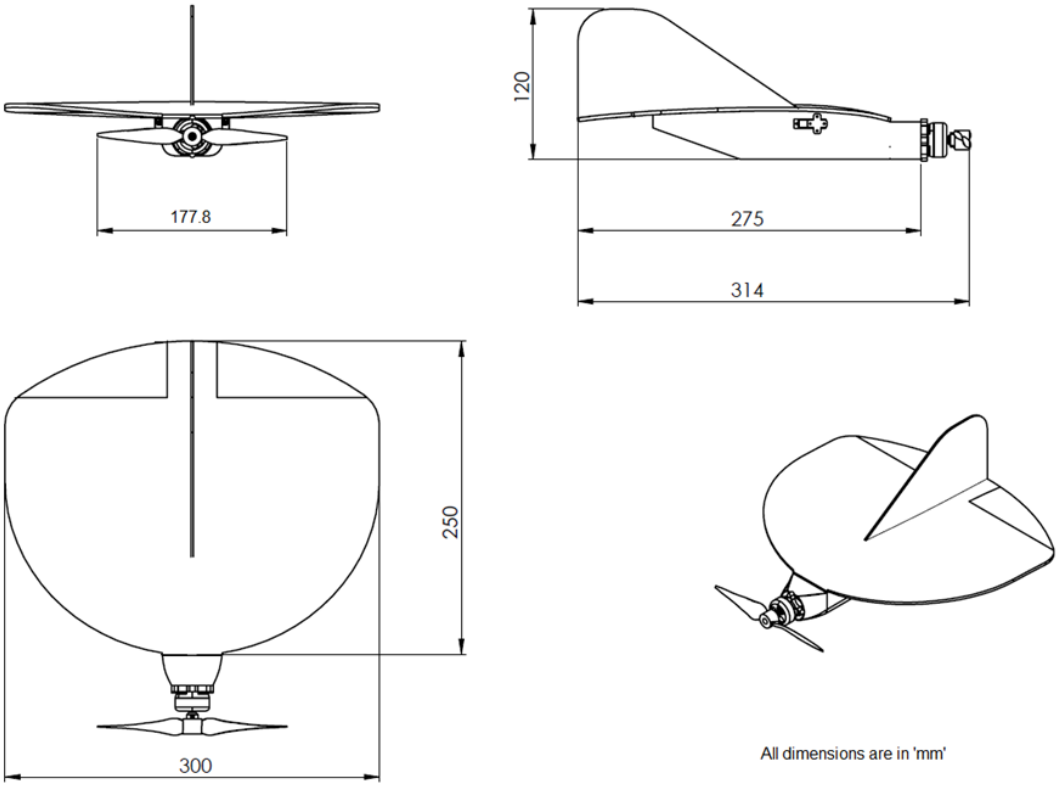

rectangular configuration with a stub front end and a boat tail at the rear.

Figure 1. Geometric details of the Test Model.

2.3 Test setup

The experiments were conducted in three phases – one on the model alone to study its airframe characteristics; the second one with the model and decoupled motor-propeller arrangement to study the characteristics of the model under the propeller induced flow; and the third on the model with attached motor-propeller arrangement.

The model was mounted on a 3-component internal strain gage balance supported by the sting-pitching sector mechanism. For testing of model with decoupled motor-propeller, the motor-propeller assembly was mounted on a different support structure from the sting without coming in contact with the model or balance. Figure 2a shows the front and side views of the experimental setup modeled in a CAD software. The support structure was an assembly of three individual components – sleeve, arm and leaf. The sleeve was mounted on the sting and provides support to the arm which extends up to the nose of the MAV model beneath the fuselage. The arm supports the leaf to which the motor was screwed. The sleeve has the provision to adjust the length of the arm. The length of the arm was adjusted on the sleeve to position the motor-propeller at a distance of 1.5 mm in front of the nose. In the flying model the motor-propeller was mounted on a splitter plate of 4.5 mm thickness which is glued to the nose. The thickness of the leaf to which the motor is screwed was 3 mm; hence 1.5 mm gap between the leaf and the model's nose was chosen so to maintain the same exact location of the motor-propeller as in flying model. The thickness of the arm is 4 mm and has a open groove on its top running along the length. The wires from the motor were taken inside the groove to the sting and outside the test section. The support assembly of the motor-propeller were cautiously designed and fabricated to cause less interference to the freestream. Figure 3 shows the experimental setup inside the test section of the tunnel. For the

third phase of test, the decoupled motor-propeller assembly was removed and the motor-propeller was mounted on a splitter plate of 4.5 mm thickness which is glued to the fuselage nose. The wires from the motor were taken inside the fuselage to the sting and outside the test section. Figure 2b shows the front and side views of the experimental setup modeled in a CAD software. The motor was powered by an external DC power supply from outside the tunnel and the speed of the propeller was controlled by Medusa Kit which was connected to the PC through Power PRO software. The motor is AXi 2203/46 (KV 1720) DC brushless motor and the propeller is a GWS 7"x3.5" propeller.

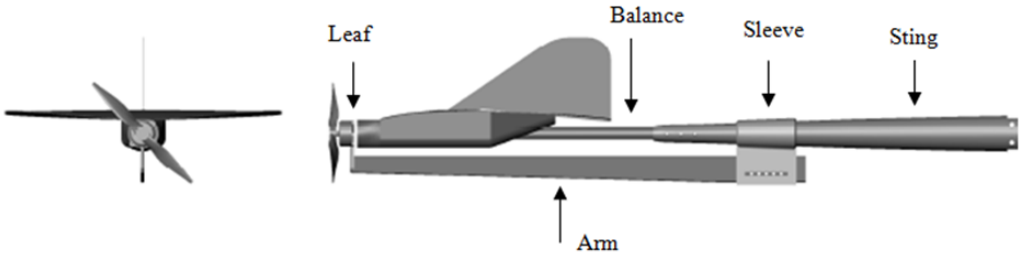

a)

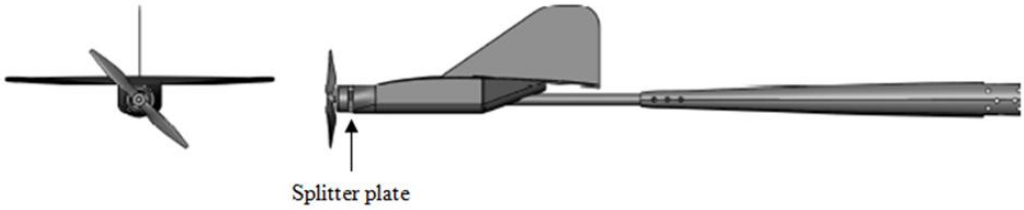

b)

Figure 2. Front & Side view of the experimental setup modeled in CAD software. a) Model with decoupled motor-propeller b) Model with attached motor-propeller

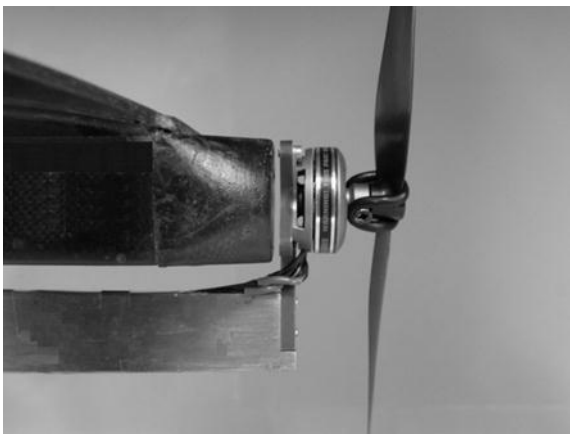

Figure 3. Experiment setup inside the test section.

All measurements on the model were done using a three component internal strain gage balance. Signals from the balance elements were amplified, digitized using 18 bit A/D converter card (NI PXI 6281) and were acquired using Labview software. The acquired data from each element was averaged and converted into forces using calibration constants of the balance. The forces and moments obtained were expressed as non-dimensional coefficients and analyzed.

2.4 Test conditions

The tests were conducted at a freestream velocity of 9 m/s. During the test, the speed of the propeller was constantly maintained at 8000 rpm for all the angles of attack, which is the steady level flight rpm of the model at this velocity. Tests were also conducted at two different propeller speeds apart from their steady level flight rpm in an incremental step of 1000 rpm to study the effects of propeller speed.

3. RESULTS AND DISCUSSION

Experiments were conducted on the model in the presence of the motor and the arm which supports the motor extending from the sting at the test velocity, prior to mounting the propeller on the motor to check whether their presence introduce any undesirable effects on the aerodynamic characteristics of the model. Figure 4 shows CAD view of the test cases undertaken to check for any undesirable effects. Figure 5 & 6 shows the comparison of lift and drag coefficients respectively with corresponding measurement uncertainties in the experiments carried out. Uncertainty in measurements is given in section C.

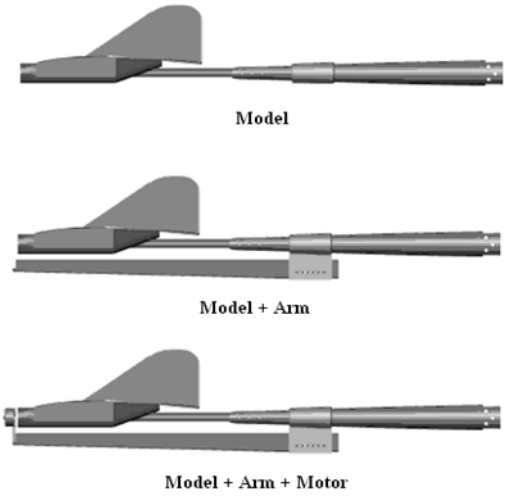

Figure 4. Schematic of test setup details.

The model in the presence of the motor and arm exhibits the same lift characteristics as the model without their presence. At higher angle of attack starting from 20^o a small drop in lift coefficient is observed and it is well within the uncertainty levels. The drag coefficient of the model in the presence of motor exhibits significantly lower drag compared to the model in the presence of arm and model alone. The drop in drag coefficient is about 8% at higher angle of attack. The decoupled motor which was right in front of the nose prevents the direct impact of the freestream on to the fuselage's nose. Hence the axial force measured by the model in this arrangement is significantly lower which contributes to a lower drag. In the following sections the lift and drag characteristics of the model in the presence of motor and arm will be taken as reference to compare with the characteristics obtained from the model under propeller induced flow at different propeller speeds.

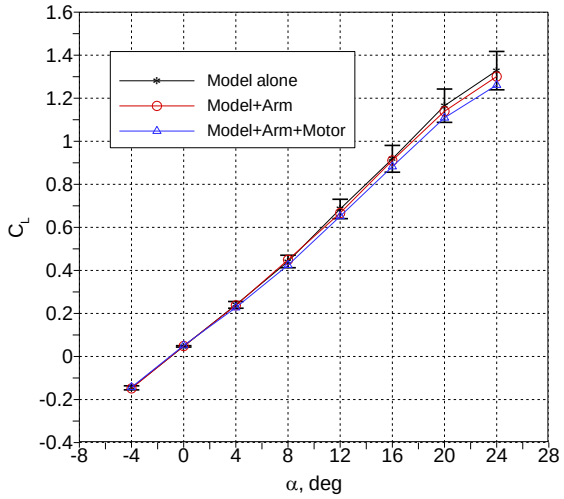

Figure. 5 Lift coefficient at $\mathbf{V}_\infty$ = 9 m/s, Re = 135000.

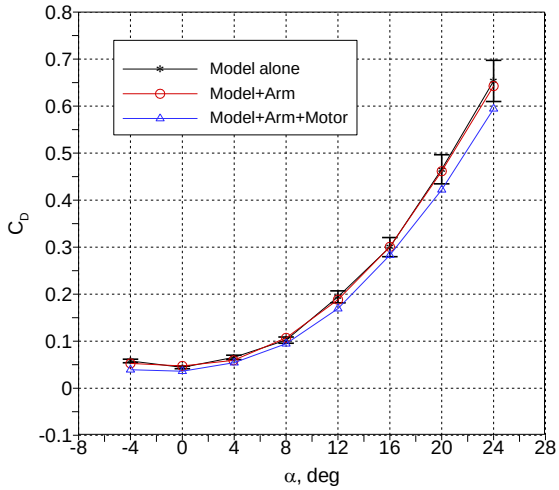

Figure 6. Drag coefficient at $\mathbf{V}_\infty$ = 9 m/s, Re = 135000.

3.1 Comparison of characteristics between model with attached motor-propeller and model with decoupled motor-propeller Test conditions

A comparison of characteristics exhibited by model with attached motor-propeller and model with decoupled motor-propeller arrangement is inevitable to justify the work carried out here. Figure 7 shows the comparison of C_D at a freestream velocity of 9 m/s and with the propeller running at 8000 rpm for both the test cases. The C_D of the model with attached motor-propeller shows lower values. In testing of model with attached motor-propeller, along the longitudinal direction of the model, the balance measures the resultant of two oppositely acting forces – the axial force experienced by the body and the thrust produced by the propeller. The resultant force measured by the balance may be positive or negative depending on the thrust produced. If the thrust dominates the axial force experienced, it would result in a negative axial force. Figure 8 compares the axial forces of the two test cases. The dominance of thrust can clearly be seen in terms of negative axial force, for the model with attached motor-propeller case. Since drag is calculated from this resultant axial force, it shows lower values. On the other hand, in testing the model with decoupled motor-propeller arrangement, the propeller induced flow is simulated over the model with the thrust produced not being measured. Hence the balance purely measures the axial force

experienced by the model under propeller induced flow. Axial forces measured are positive values as can be seen in Figure 8. Drag calculated from this measured axial force gives the actual drag value experienced by the model under propeller induced flow.

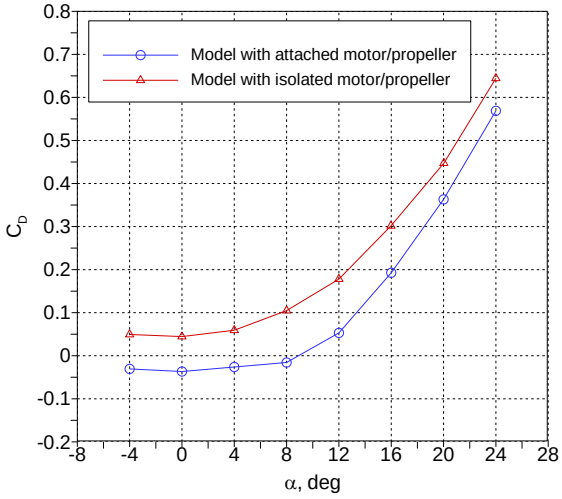

Figure 7. Drag coefficient at $\mathbf{V}_\infty$ = 9 m/s, Re = 135000.

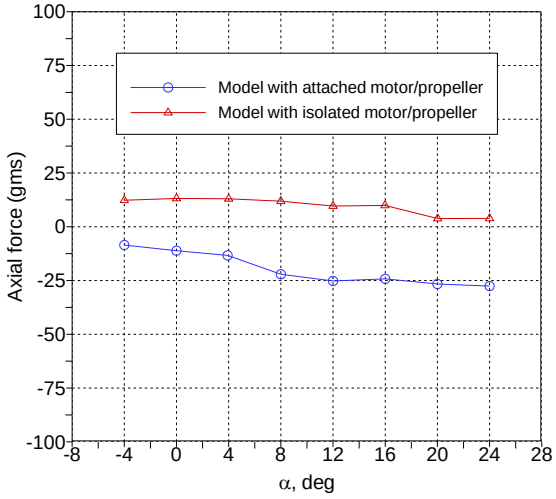

Figure 8. Axial force at $\mathbf{V}_\infty$ = 9 m/s, Re = 135000.

Figure 9 shows the comparison of C_L between the two test cases. The C_L of the model with attached motor-propeller shows higher values at higher angles of attack compared to C_L obtained from the measurement made on the decoupled motor-propeller. From Figure 10 it is seen that normal force measured is exactly same for both the test cases. The measurement of axial force for the model with attached motor-propeller not only affects the drag that is calculated, but also the lift, since lift is also a function of axial force. Though at lower angles of attack the contribution of axial force in the calculation of lift is negligible, it significantly changes the lift values at higher angles of attack which is evident from Figure 9. At lower angles of attack the C_L is same and with increase in angle of attack the difference in C_L between the two test cases progressively increases. The C_L of model with attached motor-propeller shows around 8% increase from the decoupled motor-propeller arrangement at 24^o and this difference would increase with increase in angle of attack. Hence the C_L calculated from the measured axial forces from model with attached motor-propeller testing is inaccurate at higher angles of attack.

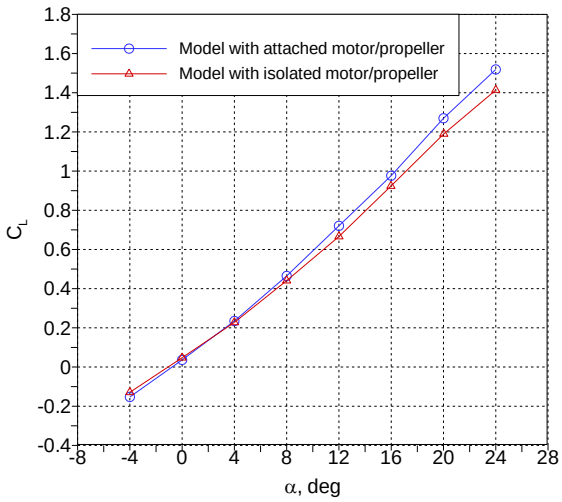

Figure 9. Lift coefficient at $\mathbf{V}_\infty$ = 9 m/s, Re = 135000.

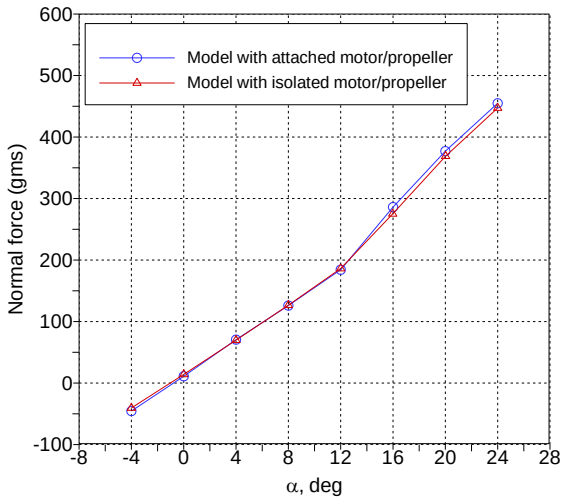

Figure 10. Normal force at V_∞ = 9 m/s, Re = 135000.

3.2 Effects of Propeller Induced flow on the aerodynamics of the Micro Air Vehicle

Figure 11 shows the comparison of lift characteristics of the model under propeller induced flow for different propeller speeds. Due to the limitations in the experimental setup the model could not be pitched more than 24^o angle of attack. The model under propeller induced flow for the different propeller speeds tested exhibits same C_L up to moderate angles of attack as the model. Starting from 16^o angle of attack the C_L of the model under propeller induced flow shows significant increase and attains a maximum of 12% to 19% at 24^o angle of attack with increase in propeller speed. The propeller induced flow creates a local acceleration of flow which increases the pressure difference between the top and bottom of the wing. This increase in the pressure difference provides extra lift to the wing.

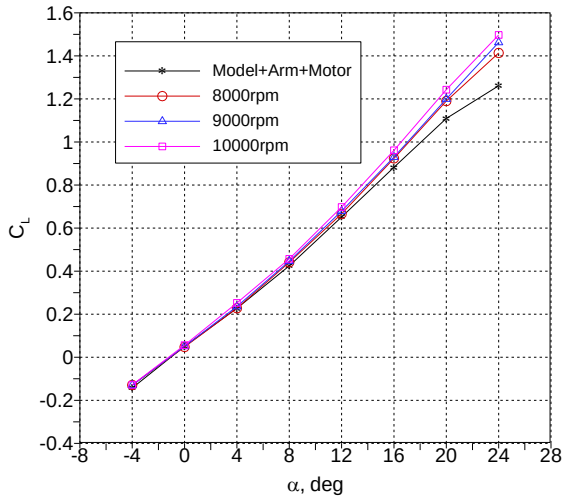

Figure 11. Lift characteristics of model under propeller-induced flow, $\mathbf{V}_\infty$ = 9 m/s, Re = 135000.

Figure 12 shows the drag characteristics of the model compared with the model under propeller induced flow at the test velocity. The model under propeller-induced flow shows substantial increase in C_D. With increase in propeller rpm, the propeller induced flow and hence the skin friction drag increases due to which there is a subsequent drag increase.

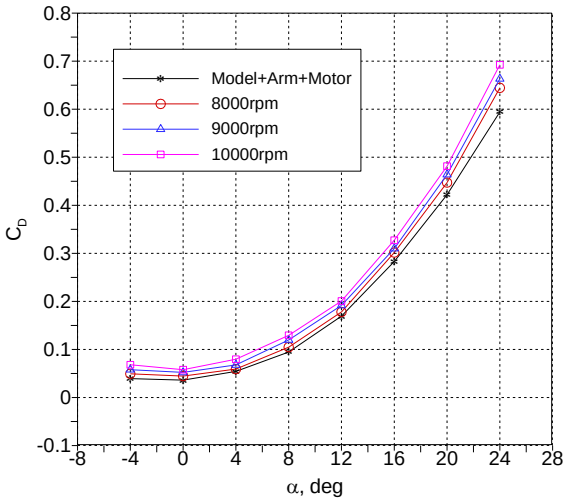

Figure 12. Drag characteristics of model under propeller-induced flow, V_∞ = 9 m/s, Re=135000.

A comparison of L/D ratios of the model with the model under propeller induced flow is shown in Figure 13. The L/D ratio peaks between 4^o and 8^o and it is in this range, a subsequent decrease in its value is observed with increase in propeller speed. This is because, with increase in propeller speed, the model exhibits same C_L up to moderate angles of attack and an increased C_D throughout the test angles of attack. This only shows that the flying vehicle cannot take any advantage with increase in the propeller rpm except to pay the drag penalty at the price of high power consumption from the battery.

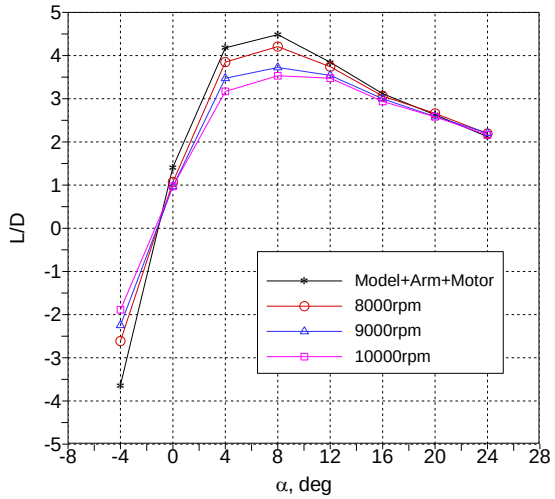

Figure 13. L/D ratio, V_∞ = 9 m/s, Re = 135000.

3.3 Uncertainty and Blockage

Uncertainties in the measurements were computed using Kline-McClintock technique [10] for error propagation. The maximum uncertainty in C_L and C_D is found to be less than 7%. The maximum blockage at 24^o angle of attack is around 8%. The coefficients presented in this work have been corrected for wind tunnel blockage according to the techniques presented by Pankhurst and Holder [11].

4. CONCLUSION

A series of experiments were conducted on a typical MAV to understand the influence of the propeller induced flow on its lift and drag characteristics. The motor-propeller arrangement was decoupled from the model and mounted in front of the model on a separate arrangement with minimal flow interference, thus the setup allows for the measurement of actual axial force experienced by the model under the propeller induced flow which enables the calculation of actual lift and drag experienced by the model. With increase in propeller rpm, C_L does not show any significant increase up to moderate angles of attack, but increase in C_D is observed throughout the test angles of attack. Thus L/D ratio of the model decreases with increase in propeller rpm up to moderate angles of attack and coalesce at higher angles of attack.

REFERENCES

[1] Null, W., Noseck, A., and Shkarayev, S., "Effects of Propulsive-Induced Flow on the Aerodynamics of Micro Air Vehicles," *23rd AIAA Applied Aerodynamic Conference*, AIAA Paper 2005-4616, Toronto, Ontario, Canada, 2005.

[2] Gamble, B., and Reeder, M., "Experimental Analysis of Propeller-Wing Interactions for a Micro Air Vehicle," *Journal of Aircraft*, Vol. 46, No.1, Jan-Feb. 2009, pp. 65–73.

[3] Arivoli, D., Dodamani, R., Antony, R., Suraj, C.S., Ramesh, G., and Ahmed, S., "Experimental Studies on a Propelled Micro Air Vehicle," *29th AIAA Applied Aerodynamics Conference*, AIAA Paper 2011-3656, Honolulu, Hawaii, June 2011.

[4] Catalano, F.M., "On the Effects of an Installed Propeller Slipstream on Wing Aerodynamic Characteristics," *ActaPolytechnica*, Vol.44, No.3, 2004.

[5] Witkowski, D., Lee, A., and Sullivan, J.P., "Aerodynamic Interaction between Propellers and Wings," *Journal of Aircraft*, Vol. 26, No.9, September 1989, pp. 829-836.

[6] Jing-Xia Zhan, Wei-jun Wang, Zhe Wu, and Jin-jun Wang, "Wind-Tunnel Experimental Investigation on a Fix-Wing Micro Air Vehicle," *Journal of Aircraft*, Vol.43, No.1, Jan-Feb 2006, pp. 279-283.

[7] Moschetta, J. M., and Thipyopas, C., "Aerodynamic Performance of a Biplane Micro Air Vehicle," *Journal of*

Aircraft, Vol.44, No.1, Jan-Feb 2007, pp. 291-299.

[8] Johnson, B., Claxton, D., Stanford, B., Jagdale, V., and Ifju, P., "Development of a Composite Bendable-Wing Micro Air Vehicle," *45th AIAA Aerospace Sciences Meeting and Exhibit*, AIAA Paper 2007-1044, Reno, Nevada, January 2007.

[9] Sudhakar, S., Kumar, C., Arivoli, D., Dodamani, R., and Venkatakrishnan, L., "Experimental Studies of Propeller Induced Flow over a Typical Micro Air Vehicle," AIAA Paper 2013-0060, Grapevine, TX, Jan. 2013.

[10] Kline, S. J., and F. A. McClintock. "Describing Uncertainties in Single-Sample Experiments," *Mechanical Engineering*, Vol. 75, No. 1, January 1953: 3-8.

[11] Pankhurst, R.C., and Holder, D.W., *Wind-Tunnel Technique*, London: Sir Isaac Pitman & Sons, Ltd., 1952.